

Adaptive Cohen's Class Time-Frequency Distribution

Manjun Cui, Zhichao Zhang, *Member, IEEE*, Jie Han, Yunjie Chen, *Member, IEEE*, and Chunzheng Cao

Abstract—The fixed kernel function-based Cohen's class time-frequency distributions (CCTFDs) allow flexibility in denoising for some specific polluted signals. Due to the limitation of fixed kernel functions, however, from the view point of filtering they fail to automatically adjust the response according to the change of signal to adapt to different signal characteristics. In this letter, we integrate Wiener filter principle and the time-frequency filtering mechanism of CCTFD to design the least-squares adaptive filter method in the Wigner-Ville distribution (WVD) domain, giving birth to the least-squares adaptive filter-based CCTFD whose kernel function can be adjusted with the input signal automatically to achieve the minimum mean-square error denoising in the WVD domain. Some examples are also carried out to demonstrate that the proposed adaptive CCTFD outperforms some state-of-the-arts in noise suppression.

Index Terms—Cohen's class time-frequency distribution, convolution, least-squares adaptive filter, mean-square error, power spectral density.

I. INTRODUCTION

COHEN'S class time-frequency distribution (CCTFD) [1], also known as the bi-linear kernel function time-frequency distribution, is one of the most representative time-frequency analysis tools of the conventional time-frequency distributions. It includes particular cases the Wigner-Ville distribution (WVD) [2], the Choi-Williams distribution [3], the Kirkwood-Rihaczek distribution [4], the Born-Jordan distribution [5], the Zhao-Atlas-Marks distribution [6], the Margenau-Hill distribution [7], and the Page distribution [8]. Indeed, it can be regarded as a unified bi-linear time-frequency distribution and has found many applications in seismic exploration, electronic countermeasures, deep-sea detection, spectral imaging, and ultrasonic inspection [9]–[14].

From the view point of signal processing, the integral form of CCTFD can be rewritten as the conventional convolution of the WVD and the kernel function. Namely, the CCTFD is a result of smoothing the WVD by using the kernel function. The main

This work was supported in part by the National Natural Science Foundation of China under Grant 61901223; in part by the Jiangsu Planned Projects for Postdoctoral Research Funds under Grant 2021K205B; in part by the Foundation of Key Laboratory of System Control and Information Processing, Ministry of Education under Grant No Scip20240121; and in part by the Foundation of Key Laboratory of Computational Science and Application of Hainan Province under Grant No JSKX202401. (*Corresponding author: Zhichao Zhang.*)

Manjun Cui, Yunjie Chen, and Chunzheng Cao are with the School of Mathematics and Statistics, Nanjing University of Information Science and Technology, Nanjing 210044, China (e-mail: cmj1109@163.com; priest-cyj@nuist.edu.cn; caochunzheng@nuist.edu.cn).

Zhichao Zhang is with the School of Mathematics and Statistics, Nanjing University of Information Science and Technology, Nanjing 210044, China, with the Key Laboratory of System Control and Information Processing, Ministry of Education, Shanghai 200240, China, and also with the Key Laboratory of Computational Science and Application of Hainan Province, Haikou 571158, China (e-mail: zzc910731@163.com).

Jie Han is with the School of Remote Sensing and Geomatics Engineering, Nanjing University of Information Science and Technology, Nanjing 210044, China (e-mail: 003645@nuist.edu.cn).

purpose the smoothing filter is not just only to suppress cross-terms of the WVD, but to achieve non-stationary signal denoising in the WVD domain, and accordingly extract the target signal from background noises or eliminate the impact of noises through the unique reconstruction property of WVD.

There are a number of attempts to use the filtering instinct of CCTFD to remove noises, giving birth to many useful and effective kernel functions of which the CCTFD works well [15]–[19]. These filtering methods employ fixed kernel functions in dealing with specific input signals, which limits the scope of applications severely. To overcome this shortcoming, it seems feasible to explore the adaptive CCTFD whose kernel function can be adjusted with the input signal automatically.

Adaptive filter is a kind of filter that is able to automatically adjust its parameters or response according to the change of signal to adapt to different signal characteristics [20]. The most celebrated result in this field is Wiener's result [21] which applies the minimum mean-square error (MSE) criterion to design the least-squares adaptive filter method. The Wiener filter has been widely used in addressing practical issues encountered frequently in radar, communications, sonar, biomedicine, and vibration engineering [22]–[28].

The core idea of this letter is to integrate Wiener filter principle and the time-frequency filtering mechanism of CCTFD to investigate the convolution type of CCTFD time-frequency analysis method. The main purpose of this letter is to design the least-squares adaptive filter method in the WVD domain, disclose the influence mechanism of the kernel function on the effect of denoising, and establish the adaptive kernel function of CCTFD with the minimum MSE in the WVD domain. The main contributions of this letter are summarized as follows:

- This letter obtains the least-squares adaptive filter in the WVD domain.
- This letter proposes the adaptive CCTFD whose kernel function takes the reversal of the least-squares adaptive filter transfer function in the WVD domain to restore signals from an extreme strong additive noise background.
- This letter demonstrates the noise suppression superiority of the proposed adaptive CCTFD over the ordinary Wiener filter and some classical fixed kernel function-based CCTFDs.

The remainder of this letter is structured as follows. In Section II, we recall some necessary background and notation on the convolution type of CCTFD. In Section III, we provide the CCTFD-based adaptive filter method for additive noises jamming signals. In Section IV, we introduce some examples to validate the effectiveness, reliability and feasibility of the proposed method. In Section V, we draw a conclusion. All the technical proofs of our theoretical results are relegated to the appendix parts.

TABLE I
SYMBOL DESCRIPTION.

Symbole	Description
T	transpose operator
—	complex conjugate operator
*	convolution operator
$\ \cdot\ _2$	L^2 -norm operator
$\mathbb{E}(\cdot)$	mathematical expectation operator
R	correlation function operator
C	CCTFD operator
W	WVD operator
\mathcal{F}	FT operator
ϕ	kernel function
Π	FT of the kernel function ϕ
H	adaptive filter in the WVD domain
σ_{MSE}^2	MSE
ε	PSD
C_g^{LSAF}	the least-squares adaptive filter-based CCTFD for the input signal g

To facilitate the understanding and clear representation of the various symbols used throughout the paper, we present Table I, which provides a detailed explanation of each symbol and its corresponding meaning.

II. CONVOLUTION TYPE OF CCTFD

The integral form of CCTFD of the function $f(\mathbf{x}) \in L^2(\mathbb{R}^N)$ reads [1], [29]

$$C_f(\mathbf{x}, \mathbf{w}) = \int_{\mathbb{R}^N} \int_{\mathbb{R}^N} \int_{\mathbb{R}^N} f\left(\mathbf{y} + \frac{\boldsymbol{\tau}}{2}\right) \overline{f\left(\mathbf{y} - \frac{\boldsymbol{\tau}}{2}\right)} \times \phi(\boldsymbol{\theta}, \boldsymbol{\tau}) e^{-2\pi i(\boldsymbol{\theta}\mathbf{x}^T + \boldsymbol{\tau}\mathbf{w}^T - \mathbf{y}\boldsymbol{\theta}^T)} d\mathbf{y} d\boldsymbol{\tau} d\boldsymbol{\theta}, \quad (1)$$

where the superscripts T and — denote the transpose operator and complex conjugate operator, respectively, and $\phi(\boldsymbol{\theta}, \boldsymbol{\tau})$ denotes the kernel function.

Let $*$ and \mathcal{F} be the conventional convolution operator and Fourier operator, respectively. Then, Eq. (1) can be rewritten as

$$C_f(\mathbf{x}, \mathbf{w}) = (W_f * \Pi)(\mathbf{x}, \mathbf{w}), \quad (2)$$

where

$$W_f(\mathbf{x}, \mathbf{w}) = \int_{\mathbb{R}^N} f\left(\mathbf{x} + \frac{\boldsymbol{\tau}}{2}\right) \overline{f\left(\mathbf{x} - \frac{\boldsymbol{\tau}}{2}\right)} e^{-2\pi i\boldsymbol{\tau}\mathbf{w}^T} d\boldsymbol{\tau} \quad (3)$$

denotes the WVD of the function $f(\mathbf{x})$, and

$$\begin{aligned} \Pi(\mathbf{x}, \mathbf{w}) &= \mathcal{F}[\phi](\mathbf{x}, \mathbf{w}) \\ &= \int_{\mathbb{R}^N} \int_{\mathbb{R}^N} \phi(\boldsymbol{\theta}, \boldsymbol{\tau}) e^{-2\pi i(\boldsymbol{\theta}\mathbf{x}^T + \boldsymbol{\tau}\mathbf{w}^T)} d\boldsymbol{\theta} d\boldsymbol{\tau} \end{aligned} \quad (4)$$

denotes the Fourier transform (FT) of the kernel function $\phi(\boldsymbol{\theta}, \boldsymbol{\tau})$. Eq. (2) indicates that the CCTFD is none other than the convolution of the WVD and the (FT version of) kernel function.

III. LEAST-SQUARES ADAPTIVE FILTER-BASED CCTFD

For a given noise polluted signal $g(\mathbf{x}) = f(\mathbf{x}) + n(\mathbf{x})$, where $f(\mathbf{x})$ and $n(\mathbf{x})$ denote the pure signal and the additive noise, respectively, the common tactic of filters is to restore the pure signal as accurately as possible, namely, find the estimate $\hat{f}(\mathbf{x})$ as close as possible to the ideal $f(\mathbf{x})$. Thanks to the convolution nature of CCTFD and the unique reconstruction property of WVD, this is equivalent to design an adaptive filter $H(\mathbf{x}, \mathbf{w})$ in the WVD domain, which can find the estimate

$$W_{\hat{f}}(\mathbf{x}, \mathbf{w}) = (W_g * H)(\mathbf{x}, \mathbf{w}) \quad (5)$$

as close as possible to the ideal $W_f(\mathbf{x}, \mathbf{w})$. According to Wiener filter principle, a natural criterion to characterize the estimation accuracy is the MSE criterion

$$\sigma_{\text{MSE}}^2 \stackrel{\text{def}}{=} \mathbb{E} \left\{ \left| W_f(\mathbf{x}, \mathbf{w}) - W_{\hat{f}}(\mathbf{x}, \mathbf{w}) \right|^2 \right\}, \quad (6)$$

where $\mathbb{E}(\cdot)$ denotes the mathematical expectation operator.

For simplicity, let $\mathbf{z} = (\mathbf{x}, \mathbf{w}) \in \mathbb{R}^{2N}$, then Eqs. (5) and (6) become

$$W_{\hat{f}}(\mathbf{z}) = (W_g * H)(\mathbf{z}) = \int_{\mathbb{R}^{2N}} W_g(\mathbf{k}) H(\mathbf{z} - \mathbf{k}) d\mathbf{k} \quad (7)$$

and

$$\sigma_{\text{MSE}}^2 = \mathbb{E} \left\{ \left| W_f(\mathbf{z}) - W_{\hat{f}}(\mathbf{z}) \right|^2 \right\}, \quad (8)$$

respectively. Now, our goal is to design an adaptive optimal filter $H_{\text{opt}}(\mathbf{z})$ in the WVD domain to minimize the MSE given by Eq. (8), or equivalently,

$$H_{\text{opt}}(\mathbf{z}) = \arg \min_{H(\mathbf{z})} \sigma_{\text{MSE}}^2. \quad (9)$$

By using the orthogonal principle [30], the stationary assumption and the conventional convolution and correlation theorems to establish, simplify and solve the Wiener-Hopf equation, respectively, the least-squares adaptive filter transfer function in the WVD domain reads

$$\mathcal{F}[H_{\text{opt}}](\mathbf{u}) = \frac{\varepsilon_{W_f, W_g}(\mathbf{u})}{\varepsilon_{W_g}(\mathbf{u})}, \quad (10)$$

where $\varepsilon_{W_f, W_g}(\mathbf{u}) = \mathcal{F}[W_f](\mathbf{u}) \overline{\mathcal{F}[W_g](\mathbf{u})}$ denotes the power spectral density (PSD) of $W_f(\mathbf{z})$ and $W_g(\mathbf{z})$, and $\varepsilon_{W_g}(\mathbf{u}) = |\mathcal{F}[W_g](\mathbf{u})|^2$ denotes the PSD of $W_g(\mathbf{z})$. Taking the inverse FT on both sides of Eq. (10) yields the least-squares adaptive filter in the WVD domain

$$H_{\text{opt}}(\mathbf{z}) = \int_{\mathbb{R}^{2N}} \frac{\varepsilon_{W_f, W_g}(\mathbf{u})}{\varepsilon_{W_g}(\mathbf{u})} e^{2\pi i\mathbf{u}\mathbf{z}^T} d\mathbf{u}. \quad (11)$$

See Appendix A for the detailed derivation of Eq. (10). Correspondingly, the minimum MSE can be reduced to zero, i.e.

$$\min_{H(\mathbf{z})} \sigma_{\text{MSE}}^2 = 0, \quad (12)$$

See Appendix B for the detailed derivation of Eq. (12).

From Eq. (4), it derives that the adaptive optimal kernel function takes the reversal of the least-squares adaptive filter transfer function in the WVD domain, i.e.,

$$\phi_{\text{opt}}(\boldsymbol{\theta}, \boldsymbol{\tau}) = \mathcal{F}[H_{\text{opt}}](-\boldsymbol{\theta}, -\boldsymbol{\tau}) = \frac{\varepsilon_{W_f, W_g}(-\boldsymbol{\theta}, -\boldsymbol{\tau})}{\varepsilon_{W_g}(-\boldsymbol{\theta}, -\boldsymbol{\tau})}. \quad (13)$$

Substituting Eq. (13) into Eq. (1) gives the least-squares adaptive filter-based CCTFD

$$\begin{aligned} &C_g^{\text{LSAF}}(\mathbf{x}, \mathbf{w}) \\ &= \int_{\mathbb{R}^N} \int_{\mathbb{R}^N} \int_{\mathbb{R}^N} g\left(\mathbf{y} + \frac{\boldsymbol{\tau}}{2}\right) \overline{g\left(\mathbf{y} - \frac{\boldsymbol{\tau}}{2}\right)} \\ &\quad \times \frac{\varepsilon_{W_f, W_g}(-\boldsymbol{\theta}, -\boldsymbol{\tau})}{\varepsilon_{W_g}(-\boldsymbol{\theta}, -\boldsymbol{\tau})} e^{-2\pi i(\boldsymbol{\theta}\mathbf{x}^T + \boldsymbol{\tau}\mathbf{w}^T - \mathbf{y}\boldsymbol{\theta}^T)} d\mathbf{y} d\boldsymbol{\tau} d\boldsymbol{\theta}. \end{aligned} \quad (14)$$

It is obvious that the transformation is designed to adapt based on the input signals f and g . This adaptability is achieved through the use of different CCTFD kernel functions, which are selected and optimized according to the characteristics of the input signals. As a result, the adaptive filter dynamically adjusts to varying signal conditions, providing a tailored and efficient filtering process that enhances the clarity and accuracy of the time-frequency representation.

IV. NUMERICAL EXPERIMENTS

This section performs four examples to verify the correctness and effectiveness of the least-squares adaptive filter method in the WVD domain. It also compares the denoising effect of the proposed adaptive CCTFD with that of the ordinary Wiener filter and some classical fixed kernel function-based CCTFDs.

In simulations, the fixed kernel functions are chosen as $\phi(\theta, \tau) = \cos\left(\frac{\theta\tau^T}{2}\right)$, $\phi(\theta, \tau) = e^{i\frac{\theta\tau^T}{2}}$, $\phi(\theta, \tau) = \frac{\sin\left(\frac{\theta\tau^T}{2}\right)}{\frac{\theta\tau^T}{2}}$ and $\phi(\theta, \tau) = e^{i\theta\|\tau\|_1}$, (here $\|\cdot\|_1$ denotes the 1-norm for vectors), corresponding to the Margenau-Hill distribution, the Kirkwood-Rihaczek distribution, the Born-Jordan distribution and the Page distribution, respectively. For simplicity, we call the filtering methods using fixed kernel functions $\cos\left(\frac{\theta\tau^T}{2}\right)$, $e^{i\frac{\theta\tau^T}{2}}$, $\frac{\sin\left(\frac{\theta\tau^T}{2}\right)}{\frac{\theta\tau^T}{2}}$ and $e^{i\theta\|\tau\|_1}$ as Margenau-Hill, Kirkwood-Rihaczek, Born-Jordan and Page, respectively.

Example 1 (Linear frequency-modulated (LFM) signal): The polluted signal is selected for the LFM signal $e^{2\pi i\left(x + \frac{x^2}{2}\right)}$.

Example 2 (Gaussian enveloped LFM (GELFM) signal): The polluted signal is selected for the GELFM signal $e^{-\frac{(x+1)^2}{8}} e^{2\pi i x^2}$.

Example 3 (Quadratic frequency-modulated (QFM) signal): The polluted signal is selected for the QFM signal $e^{2\pi i\left(-3x + \frac{x^2}{2} + \frac{x^3}{4}\right)}$.

Example 4 (Sinusoidal frequency-modulated (SFM) signal): The polluted signal is selected for the SFM signal $e^{i[1.3\pi x + 2 \sin(0.6\pi x)]}$.

In examples 1–4, additive white Gaussian noise is introduced to the signals, with the SNR ranging from -5 dB to 5 dB and the observation interval is set to $[-5s, 5s]$. The sampling frequencies are set as follows: 80 Hz for example 1, 100 Hz for example 2, 150 Hz for example 3 and 175 Hz for example 4.

Figs. 1(a) and (b) plot respectively the SNR-MSE (logarithm base 10) and SNR-peak SNR (PSNR) (average of real and imaginary parts) line charts of the estimated LFM signal using six filtering methods including Margenau-Hill, Kirkwood-Rihaczek, Born-Jordan, Page, Wiener filter and the proposed adaptive CCTFD. Figs. 2(a) and (b) plot respectively the SNR-MSE and SNR-PSNR line charts of the estimate GELFM signals using these six filtering methods. Figs. 3(a) and (b) plot respectively the SNR-MSE and SNR-PSNR line charts of the estimate QFM signals using these six filtering methods. Figs. 4(a) and (b) plot respectively the SNR-MSE and SNR-PSNR line charts of the estimate SFM signals using these six filtering methods. It can be seen that the proposed adaptive CCTFD achieves better noise suppression performance than Margenau-Hill, Kirkwood-

Rihaczek, Born-Jordan, Page, and Wiener filters under different SNR levels.

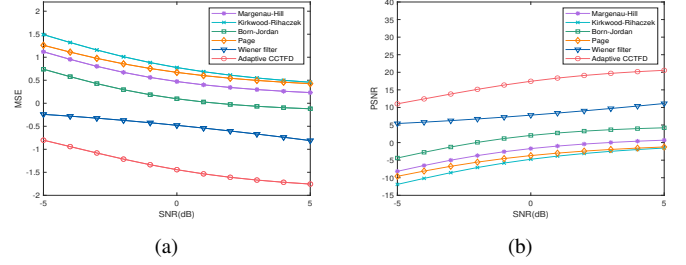


Fig. 1. Performance evaluation of six denoising methods for the LFM signal at SNR levels from -5 dB to 5 dB under white Gaussian noise: (a) MSE performance of the estimated LFM signals; (b) PSNR performance of the estimated LFM signals.

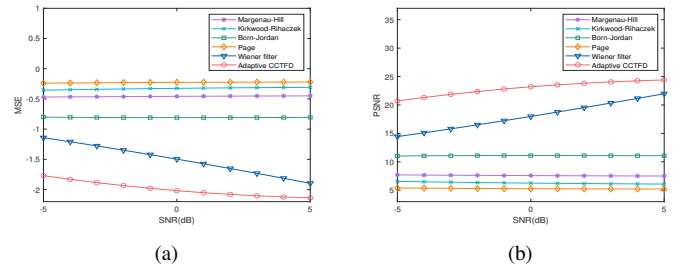


Fig. 2. Performance evaluation of six denoising methods for the GELFM signal at SNR levels from -5 dB to 5 dB under white Gaussian noise: (a) MSE performance of the estimated GELFM signals; (b) PSNR performance of the estimated GELFM signals.

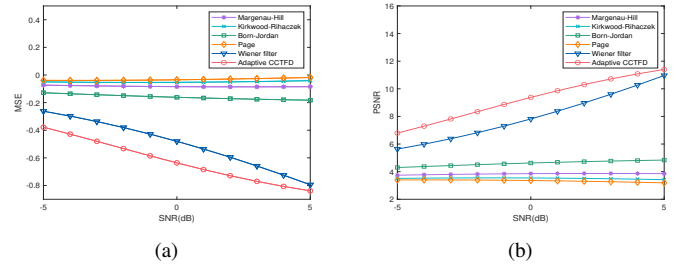


Fig. 3. Performance evaluation of six denoising methods for the QFM signal at SNR levels from -5 dB to 5 dB under white Gaussian noise: (a) MSE performance of the estimated QFM signals; (b) PSNR performance of the estimated QFM signals.

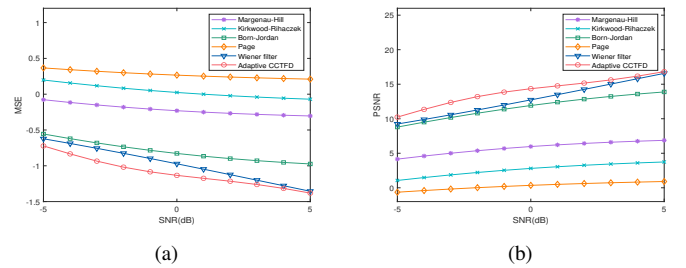


Fig. 4. Performance evaluation of six denoising methods for the SFM signal at SNR levels from -5 dB to 5 dB under white Gaussian noise: (a) MSE performance of the estimated SFM signals; (b) PSNR performance of the estimated SFM signals.

Additionally, we investigated the denoising performance of the six methods under conditions of different colored noise. The four

TABLE II
THE MSE AND PSNR OF SIX FILTERING METHODS UNDER DIFFERENT
COLORED NOISE CONDITIONS.

Example	LFM	GELFM	QFM	SFM	
MSE (Mean-Square Error)					
Pink noise	Margenau-Hill	-0.0016	-0.1592	-0.0513	-0.1319
	Kirkwood-Rihaczek	0.0676	-0.0050	-0.0330	-0.1200
	Born-Jordan	-0.1582	-0.3053	-0.1123	-0.2134
	Page	0.0996	-0.0360	-0.0201	-0.0582
	Wiener filter	-0.4985	-0.6911	-0.4699	-0.4268
	Adaptive CCTFD	-1.5318	-0.9807	-0.3169	-0.3369
Blue noise	Margenau-Hill	0.1437	-0.4563	-0.0637	-0.3730
	Kirkwood-Rihaczek	0.3580	-0.3711	0.0063	-0.2404
	Born-Jordan	-0.1057	-0.5265	-0.2016	-0.9358
	Page	0.3281	-0.3355	0.0239	0.0682
	Wiener filter	-0.4676	-0.6632	-0.5208	-1.0831
	Adaptive CCTFD	-1.2999	-0.9581	-0.7917	-1.6128
Red noise	Margenau-Hill	0.0655	-0.3004	-0.0624	-0.2233
	Kirkwood-Rihaczek	0.1243	-0.2567	-0.0475	-0.2145
	Born-Jordan	-0.0907	-0.3810	-0.1369	-0.3623
	Page	0.1720	-0.2790	-0.0082	-0.0851
	Wiener filter	-0.8039	-1.2798	-0.9489	-0.7804
	Adaptive CCTFD	-1.7448	-1.3028	-0.4032	-0.3919
PSNR (Peak Signal-to-Noise Ratio)					
Pink noise	Margenau-Hill	3.0323	5.2766	3.5237	4.3306
	Kirkwood-Rihaczek	2.3400	3.7410	3.3431	4.2110
	Born-Jordan	4.6190	7.0716	4.1339	5.1494
	Page	2.0433	3.7370	3.2109	3.5963
	Wiener filter	8.8314	10.3192	8.0556	7.8716
	Adaptive CCTFD	18.5390	12.8503	6.1978	6.5799
Blue noise	Margenau-Hill	1.5865	7.6228	3.6468	7.2377
	Kirkwood-Rihaczek	-0.5454	6.8108	2.9469	5.4278
	Born-Jordan	4.1557	8.3757	5.0342	13.0179
	Page	-0.2493	6.4764	2.7708	2.3297
	Wiener filter	8.1082	9.8937	8.6899	14.4000
	Adaptive CCTFD	16.0114	12.6000	10.9354	19.6753
Red noise	Margenau-Hill	2.3888	6.3998	3.6360	5.2562
	Kirkwood-Rihaczek	1.7774	5.9456	3.4881	5.1559
	Born-Jordan	4.0111	7.4167	4.3805	6.6348
	Page	1.3606	5.9863	3.0925	3.8628
	Wiener filter	11.8832	16.7052	13.1156	11.9071
	Adaptive CCTFD	20.4654	16.1495	7.0496	7.2056

signals were subjected to various types of colored noise: pink noise, blue noise, and red noise. The observation interval is set to $[-5s, 5s]$, and the sampling frequencies are set as follows: 30Hz for example 1, 50Hz for example 2, 150Hz for examples 3 and 4. Table II presents the MSE and PSNR values of the output signals through the six filters under the influence of three types of colored noise. It can be seen that for blue noise, our proposed adaptive CCTFD significantly outperforms the other methods. For pink and red noise, our method is superior to the others for LFM and GELFM signals (except for the PSNR value of red noise in the GELFM signal, which is slightly lower than that of the Wiener filter). For pink and red noise, the Wiener filter performs better than ours for QFM and SFM signals. However, overall, our method consistently outperforms the fixed kernel function filtering methods.

V. CONCLUSION

The convolution type of CCTFD time-frequency analysis method suitable for the adaptive filter denoising for additive noises jamming signals under the condition of low SNR was established, giving rise to the adaptive kernel function which minimizes the MSE in the WVD domain. The proposed adaptive CCTFD can automatically adjust its kernel function according to the change of signal to adapt to different signal characteristics. It turns out that its denoising effect is better than that of some classical fixed kernel function-based CCTFDs, including the Margenau-Hill distribution, the Kirkwood-Rihaczek distribution, the Born-Jordan distribution, and the Page distribution. Under

white Gaussian noise, our method outperforms the ordinary Wiener filter, while under colored noise, it performs comparably to the Wiener filter.

APPENDIX

In this section, we prove all the theoretical results in the letter.

A. Proof of Eq. (10)

By using the orthogonal principle

$$\mathbb{E} \left\{ [W_f(z) - (W_g * H_{\text{opt}})(z)] \overline{W_g(z')} \right\} = 0, z' \in \mathbb{R}^{2N}, \quad (\text{A.1})$$

we establish the Wiener-Hopf equation

$$R_{W_f, W_g}(z, z') - \int_{\mathbb{R}^{2N}} R_{W_g}(k, z') H_{\text{opt}}(z - k) dk = 0, \quad (\text{A.2})$$

where R_{W_f, W_g} denotes the cross-correlation function between W_f and W_g , and R_{W_g} denotes the auto-correlation function of W_g . In general, we can obtain H_{opt} by solving Eq. (A.2) numerically. Particularly, if W_f and W_g are stationary, Eq. (A.2) simplifies to

$$R_{W_f, W_g}(z - z') - \int_{\mathbb{R}^{2N}} R_{W_g}(k - z') H_{\text{opt}}(z - k) dk = 0. \quad (\text{A.3})$$

Taking the change of variables $z - z' = p$ and $z - k = q$ yields

$$R_{W_f, W_g}(p) - \int_{\mathbb{R}^{2N}} R_{W_g}(p - q) H_{\text{opt}}(q) dq = 0. \quad (\text{A.4})$$

Thanks to the conventional convolution and correlation theorems, we solve Eq. (A.4) to obtain

$$\mathcal{F}[W_f](u) \overline{\mathcal{F}[W_g](u)} = \mathcal{F}[H_{\text{opt}}](u) |\mathcal{F}[W_g](u)|^2, \quad (\text{A.5})$$

and therefore, we arrive the required result (10). ■

B. Proof of Eq. (12)

The minimize MSE takes

$$\min_{H(z)} \sigma_{\text{MSE}}^2 = \mathbb{E} \left\{ [W_f(z) - (W_g * H_{\text{opt}})(z)] \overline{W_f(z)} \right\}. \quad (\text{B.1})$$

Similar to Eqs. (A.2)–(A.4), we have

$$\min_{H(z)} \sigma_{\text{MSE}}^2 = R_{W_f}(0) - \int_{\mathbb{R}^{2N}} R_{W_g, W_f}(-k) H_{\text{opt}}(k) dk. \quad (\text{B.2})$$

Because of Parseval's relation of the WVD, it follows that

$$R_{W_f}(0) = \int_{\mathbb{R}^{2N}} |W_f(z)|^2 dz = \|f\|_2^4. \quad (\text{B.3})$$

Thanks to the conventional convolution and correlation theorems, substituting Eq. (10) yields

$$\begin{aligned} & \int_{\mathbb{R}^{2N}} R_{W_g, W_f}(-k) H_{\text{opt}}(k) dk \\ &= \int_{\mathbb{R}^{2N}} \mathcal{F}[H_{\text{opt}}](u) \mathcal{F}[W_g](u) \overline{\mathcal{F}[W_f](u)} du \\ &= \int_{\mathbb{R}^{2N}} \frac{\varepsilon_{W_f, W_g}(u) \varepsilon_{W_g, W_f}(u)}{\varepsilon_{W_g}(u)} du. \end{aligned} \quad (\text{B.4})$$

With Eqs. (B.2), (B.3) and (B.4), we have

$$\min_{H(z)} \sigma_{\text{MSE}}^2 = \|f\|_2^4 - \int_{\mathbb{R}^{2N}} \frac{\varepsilon_{W_f, W_g}(u) \varepsilon_{W_g, W_f}(u)}{\varepsilon_{W_g}(u)} du. \quad (\text{B.5})$$

By further simplifying the above equation, we arrive the required result (12). ■

REFERENCES

- [1] L. Cohen, *Time-Frequency Analysis: Theory and Applications*. Upper Saddle River, NJ, USA: Prentice Hall, 1995.
- [2] E. Wigner, "On the quantum correction for thermodynamic equilibrium," *Phys. Rev.*, vol. 40, no. 5, pp. 749–759, Jun. 1932.
- [3] P. Zhao and L. Xu, "Research on time domain filtering based on Choi-Williams distribution about time-phase modulation," in *Proc. 2021 7th Annual International Conference on Network and Information Systems for Computers (ICNISC)*. Guiyang, China: IEEE, Jul. 2021, pp. 708–715.
- [4] A. Rihaczek, "Signal energy distribution in time and frequency," *IEEE Trans. Inf. Theory*, vol. 14, no. 3, pp. 369–374, May 1968.
- [5] G. Quan, T. Jie, S. Huan, and W. Hong, "A novel time-frequency distribution for the short-time signal," in *Proc. 2021 4th International Conference on Information Communication and Signal Processing (ICICSP)*. Shanghai, China: IEEE, Sep. 2021, pp. 130–133.
- [6] Y. Zhao, L. E. Atlas, and R. J. Marks, "The use of cone-shaped kernels for generalized time-frequency representations of nonstationary signals," *IEEE Trans. Signal Process.*, vol. 38, no. 7, pp. 1084–1091, Jul. 1990.
- [7] C. Liang, Q. Bai, Y. Wang, Y. Gao, H. Zhang, and B. Jin, "Spatial resolution enhancement in OFDR using Margenau Hill spectrogram," *J. Light. Technol.*, Jan. 2024, doi: 10.1109/JLT.2024.3352614.
- [8] X. Xia, Y. Owechko, B. H. Soffer, and R. M. Matic, "On generalized-marginal time-frequency distributions," *IEEE Trans. Signal Process.*, vol. 44, no. 11, pp. 2882–2886, Nov. 1996.
- [9] J. Brynolfsson, I. Reinhold, and M. Sandsten, "A time-frequency-shift invariant parameter estimator for oscillating transient functions using the matched window reassignment," *Signal Process.*, vol. 183, p. 107913, Jun. 2021.
- [10] Q. Wang, Y. Li, S. Chen, and B. Tang, "Matching demodulation synchrosqueezing S transform and its application in seismic time-frequency analysis," *IEEE Geosci. Remote. Sens. Lett.*, vol. 19, pp. 1–5, Jan. 2021.
- [11] S. Xu, L. Liu, and Z. Zhao, "DTFTNet: Radar modulation recognition with deep time-frequency transformation," *IEEE Trans. Cogn. Commun. Netw.*, vol. 9, no. 5, pp. 1200–1210, May 2023.
- [12] A. L. O. Vitor, A. Goedel, M. F. Castoldi, W. A. Souza, and G. H. Bazan, "Induction machine fault diagnosis with quadratic time-frequency distributions: State of the art," *IEEE Trans. Instrum. Meas.*, vol. 72, pp. 1–16, Oct. 2023.
- [13] X. Han, M. Liu, S. Zhang, R. Zheng, and J. Lan, "A passive DOA estimation algorithm of underwater multipath signals via spatial time-frequency distributions," *IEEE Trans. Veh. Technol.*, vol. 70, no. 4, pp. 3439–3455, Mar. 2021.
- [14] J. Ding, F. Deng, Q. Liu, and J. Wang, "Regional forecasting of significant wave height and mean wave period using EOF-EEMD-SCINet hybrid model," *Appl. Ocean Res.*, vol. 136, p. 103582, Jul. 2023.
- [15] Z. Qu, C. Hou, C. Hou, and W. Wang, "Radar signal intra-pulse modulation recognition based on convolutional neural network and deep Q-learning network," *IEEE Access*, vol. 8, pp. 49 125–49 136, Mar. 2020.
- [16] Y. Yao, Y. Lu, X. Zhang, F. Wang, and R. Wang, "Reducing trade-off between spatial resolution and frequency accuracy in BOTDR using Cohen's class signal processing method," *IEEE Photon. Technol. Lett.*, vol. 24, no. 15, pp. 1337–1339, Jun. 2012.
- [17] N. Lopac, F. Hrzic, I. P. Vuksanovic, and J. Lerga, "Detection of non-stationary GW signals in high noise from Cohen's class of time-frequency representations using deep learning," *IEEE Access*, vol. 10, pp. 2408–2428, Dec. 2021.
- [18] P. Jadhav and S. Mukhopadhyay, "Automated sleep stage scoring using time-frequency spectra convolution neural network," *IEEE Trans. Instrum. Meas.*, vol. 71, pp. 1–9, May 2022.
- [19] Y. Li, X. Zhang, Z. Chen, Y. Yang, C. Geng, and M. Zuo, "Time-frequency ridge estimation: An effective tool for gear and bearing fault diagnosis at time-varying speeds," *Mech. Syst. Sig. Process.*, vol. 189, p. 110108, Apr. 2023.
- [20] P. S. R. Diniz, *Adaptive Filtering*. Berlin, Germany: Springer, 1997.
- [21] N. Wiener, *Extrapolation, Interpolation, and Smoothing of Stationary Time Series: with Engineering Applications*. New York, USA: The MIT press, 1949.
- [22] M. Ceccato, F. Formaggio, and S. Tomasin, "Spatial GNSS spoofing against drone swarms with multiple antennas and Wiener filter," *IEEE Trans. Signal Process.*, vol. 68, pp. 5782–5794, Oct. 2020.
- [23] J. Y. Baudais, S. Meric, B. Benmeziene, and K. Cinglant, "Doppler robustness of joint communication and radar systems using the Wiener filter," *IEEE Trans. Commun.*, vol. 71, no. 8, May 2023.
- [24] D. Plabst, F. J. G. Gomez, T. Wiegart, and N. Hanik, "Wiener filter for short-reach fiber-optic links," *IEEE Commun. Lett.*, vol. 24, no. 11, pp. 2546–2550, Jul. 2020.
- [25] H. Song, S. Sasada, N. Masumoto, T. Kadoya, M. Okada, K. Arihiro, X. Xiao, and T. Kikkawa, "A two-stage rotational surface clutter suppression method for microwave breast imaging with multistatic impulse-radar detector," *IEEE Trans. Instrum. Meas.*, vol. 69, no. 12, pp. 9586–9598, Jun. 2020.
- [26] S. Y. Chang and H. C. Wu, "Tensor Wiener filter," *IEEE Trans. Signal Process.*, vol. 70, pp. 410–422, Jan. 2022.
- [27] C. Qi, J. Lin, Y. Wu, and F. Gao, "A Wiener model identification for creep and vibration linear and hysteresis nonlinear dynamics of piezoelectric actuator," *IEEE Sens. J.*, vol. 21, no. 24, pp. 27 570–27 581, Nov. 2021.
- [28] Y. Vered and S. Elliott, "A parallel analog and digital adaptive feedforward controller for active noise control," *IEEE/ACM Trans. Audio, Speech, Language Process.*, vol. 32, pp. 1100–1108, Jan. 2024.
- [29] H. M. Ozaktas, N. Erkaya, and M. A. Kutay, "Effect of fractional Fourier transformation on time-frequency distributions belonging to the Cohen class," *IEEE Signal Process. Lett.*, vol. 3, no. 2, pp. 40–41, Feb. 1996.
- [30] J. Proakis, "Probability, random variables and stochastic processes," *IEEE Trans. Acoust., Speech, Signal Process.*, vol. 33, no. 6, pp. 1637–1637, Dec. 1985.